Steel and Composite Structures, *Vol. 22, No. 6 (2016) 1465-1486*
DOI: http://dx.doi.org/10.12989/scs.2016.22.6.1465

Experimental study on shear behavior of I-girder with concrete-filled tubular flange and corrugated web

Y.B. Shao * and Y.M. Wang

School of Mechatronic Engineering, Southwest Petroleum University, Xindu Road 8#, Xindu District, Chengdu 610500, P.R. China

(*Received August 24, 2016, Revised November 22, 2016, Accepted December 01, 2016*)

Abstract. Conventional plate I-girders are sensitive to local buckling of the web when they are subjected mainly to shear action because the slenderness of the web in out-of-plane direction is much bigger. The local buckling of the web can also cause the distorsion of the plate flange under compression as a thin-walled plate has very low torsional stiffness due to its open section. A new I-girder consisted of corrugated web, a concrete-filled rectangular tubular flange under compression and a plate flange under tension is presented to improve its resistance to local buckling of the web and distorsion of the flat plate flange under compression. Experimental tests on a conventional plate I-girder and a new presented I-girder are conducted to study the failure process and the failure mechanisms of the two specimens. Strain developments at some critical positions, load-lateral displacement curves, and load-deflection curves of the two specimens have all be measured and analyzed. Based on these results, the failure mechanisms of the two kinds of I-girders are discussed.

Keywords: I-girder; shear behavior; corrugated web; concrete-filled tubular flange; failure mechanism

1. Introduction

Steel I-girder is a very common flexural member used in building and bridge engineering. The conventional I-girder is consisted of two flat-plate flanges and a flat-plate web. In a flexural member with a large span or subjected to a large load, the I-girder is generally designed with a certain height for resisting the moment, which causes the web to be very slender. A slender web is very sensitive to buckling due to its weak bending stiffness in out-of plane direction. To avoid such buckling, transverse or longitudinal stiffeners are placed to the web. The placement of the stiffeners produces two disadvantages: Firstly, the stiffeners definitely raise the overall self-weight of the I-girder, and the amount of the steel material is increased. Secondly, all the stiffeners are necessary to be connected to the flanges and to the web through welding. The welding process can generate high residual stress, and it causes the region around the weld to become brittle, which is especially harmful to the behavior of the member under fatigue and seismic action.

In recent years, corrugated web is presented and used in many building and bridge structures due to its various advantages, in which three most attractive ones are light weight, high out-of-plane bending stiffness and long fatigue life. As the web plate is corrugated, it has a certain height

*Corresponding author, Ph.D., Professor, E-mail: ybshao@swpu.edu.cn

 ISSN: 1229-9367 (Print), 1598-6233 (Online)

in out-of-plane direction. The height of the corrugation is much bigger than the web thickness, and hence the out-of-plane bending stiffness of the web is improved efficiently. Because of this reason, the thickness of the web can be designed with a very small value (1 mm ~ 3 mm). The small thickness makes the self-weight of the web very slight. Simultaneously, the high out-of-plane bending stiffness of the corrugated web can improve the resistance to buckling. Finally, the corrugated web has a much longer fatigue life than the flat-plate web with welded stiffeners because the residual stress caused by welding process between the stiffeners and the web is avoided in the corrugated web.

Research studies on corrugated web in I-girders have been carried out by many researchers in the past two decades. In the studies on the shear resistance of corrugated web, Elgaaly *et al*. (1996) conducted experimental test on steel beams with corrugated web under shear action, and the tested results indicated that the failure mode of the steel beams was buckling of the web. They also presented finite element modeling method for studying the detailed failure mechanism for steel beams with corrugated web. Equations for predicting the local and the global buckling of the corrugated web were proposed. Luo and Edlund (1995, 1996a, b) investigated the factors influencing the shear resistance and the post-buckling of steel beams with trapezoidally corrugated web. Driver *et al*. (2006) studied the effect of imperfection of the corrugated web on the buckling load, and corrected equations considering such effect were presented for engineering design. Yi *et al*. (2008) summarized the possible buckling failures of corrugated web under shear action, and the influencing factors on the local, global and interactive buckling modes were also analyzed. Sause and Braxtan (2011) presented new equations for predicting the shear resistance of corrugated web by considering the interaction among different buckling modes. Guo and Sause (2014) proposed equations for calculating the local buckling resistance for trapezoidally corrugated web under shear action.

In the investigations on the flexural behavior of corrugated web in steel beams, Elgaaly *et al*. (1997) found from experimental tests that the corrugated web has very little contribution to the bending resistance of steel beams and it mainly sustains the shear action. The maximum bending moment for a steel beam with corrugated web can be estimated from the yielding strength of the two flanges. Basher *et al*. (2011) studied the flexural behavior of curved composite plate girders with trapezoidally corrugated web through finite element simulation, and some empirical methods for estimating the static strength were presented. Abbas *et al*. (2006, 2007) found that out-of-plane torsional action exists in the flanges for steel beams with corrugated web under in-plane bending moment, and they suggested that such torsion can be analyzed by assuming that the flanges are subjected to transverse bending action. Sayed-Ahmed (2005) concluded that steel I-beams with corrugated web have a higher resistance to flexural-torsional buckling than conventional steel I-beams. Moon *et al*. (2009) and Nguyen *et al*. (2010) studied the flexural-torsional behavior of steel I-beams with corrugated web under pure bending moment, and they presented the location of the shear center and a new wrapping constant. Ibrahim (2014) analyzed the flexural-torsional behavior of unsymmetrical plate girders with trapezoidally corrugated web, and a new wrapping constant and the shear center were both presented.

For the local bearing capacity of steel beams with corrugated web under patch loading, some researchers also carried out many studies. Luo and Edlund (1996a) analyzed the ultimate strength of steel beams with trapezoidally corrugated webs under patch loading through numerical simulation and parametric study. Elgaaly and Seshadri (1997) conducted experimental tests on several steel beams with corrugated web under partial compressive edge loading, and it was found from the experimental observations that web buckling and web yielding were two dominant failure

modes in the specimens. Kövesdi *et al*. (2010) analyzed the factors influencing the local bearing capacity of steel beams with corrugated web based on the reported experimental results and some reported design equations.

As mentioned previously, the corrugated webs can avoid the placement of stiffeners, and hence a steel beam with corrugated web is advantageous for resisting fatigue loading. Machacek and Tuma (2006) investigated the fatigue behavior of steel beams with corrugated web through finite element analyses by considering the imperfection and nonlinearity. Ibrahim *et al*. (2006) studied the performance of steel girders with trapezoidally corrugated web under monotonic and cyclic loading, and they provided the relationship between the stress range and the loading cycles.

Because the corrugated web can improve the out-of-plane bending stiffness, the steel beams with corrugated web are able to be designed with a large height. However, a very high beam is very weak for preventing global instability when it is subjected to lateral loading. Additionally, the local buckling of the web produces an out-of-plane rotation, which can also cause the plate flange to have a rotating deformation because the open section has a low torsional stiffness. To improve the resistance to torsional deformation of the flange, some researchers presented a new method by using hollow section tube to replace the conventional flat-plate flange. This method is based on the fact that a closed section (hollow section tubular flange) has a much larger torsional stiffness compared to an open section (flat-plate flange). Heldt and Mahendran (1997) studied the lateral-distorsional buckling of hollow flange beams under pure bending, and they obtained the theoretical equations for predicting the static strength. Avery *et al*. (2000) presented the finite element model to carry out nonlinear analyses for studying the flexural capacity of hollow flange beams. Kurniawan and Mahendran (2009) analyzed the elastic buckling of simply supported LiteSteel beams (LSB) subjected to transverse loading through finite element analyses, and some suggestions were proposed. Dong and Sause (2009) analyzed steel beams with tubular flange by using finite element method considering material nonlinearity, initial imperfection and residual stresses. Hassanein and Kharoob (2010, 2012) investigated the shear behavior of steel beams with two square hollow section tubular flanges and plate webs with stiffeners. Based on the investigations, they proposed revised equations for estimating the shear strength. Anapayan *et al*. (Anapayan *et al*. 2011, Anapayan and Mahendran 2012) studied a channel beam with two tubular flanges through experimental tests, and they suggested the design method for calculating the flexural strength and the flexural-torsional buckling of this new beam. Hassanein and Silvestre (2013) analyzed the different flexural resistances of the hollow tubular flange plate girders and conventional plate girders in case that the web is un-stiffened and slender. The results indicate that the girders with hollow tubular flange have higher value of the critical bending moment at buckling.

Although hollow tubular flange girders have much higher capacity to resist global instability, the flange is much sensitive to local buckling due to its thin-wall tube and hollow section. Such local buckling causes the tubular flange to fail far before its flexural yielding strength, which can not develop the potential of high yield strength for steel materials. To avoid this phenomenon, the tubular flange can be filled with concrete. The concrete has relatively higher compressive strength and it can also avoid the transverse deformation of the tube efficiently. Based on this idea, Sause *et al*. (2008) presented a new girder by using concrete-filled tubular flange to replace conventional flat-plate flange, and they carried out some experimental tests to assess the performance of this new girder. Experimental results showed that the global stability of the new girder was higher than that of conventional plate girders. Gao *et al*. (2014) studied the flexural behavior of I-girders with concrete-filled pentagonal flange through experimental tests. The results showed that the global

buckling of the I-girders was prevented efficiently. Based on previous studies, Sause (2015) studied the application of this new beam on curved flexural members. Through experimental tests, it was found that the beams with concrete-filled tubular flange were more suitable for curved members due to their much higher torsional stiffness.

Since corrugated web can improve the resistance to local buckling and concrete-filled tubular flange can prevent distorsional deformation, a new type I-girder with corrugated web and concrete-filled tubular flange is expected to combine the two advantages. This study is carried out to investigate the shear behavior of a short new I-girder under three-point loading.

2. Experimental test

2.1 Test specimens

The new I-girder in the test is consisted of corrugated web, a concrete-filled tubular flange and a flat-plate flange, as shown in Fig. 1. In the experimental test, the span of the new I-girder is designed to be small, and a concentrated load is applied at the mid-span. In this case, the I-girder is mainly subjected to shear action. It is also specified here that the bottom flange in the I-girder, as shown in Fig. 1, is a flat-plate, and it is not a concrete-filled tube. The I-girder is designed to have hinged boundary conditions at both of its ends in the experimental test to simulate the I-girders used in bridge engineering. In a hinged connection, the rotation is not restricted, and the bottom flange is under tension while the top flange is subjected to compression when the I-girder is subjected to bending moment. As the resistance to global instability of a steel beam is mainly determined by the lateral and torsional stiffness of the compressed flange, the top flange is designed to be a concrete-filled tubular one while the bottom flange under tension is designed to be a flat plate. For the web, trapezoidally corrugated plate is used as shown in Fig. 1.

To compare the different performances of the new I-girder and the conventional plate I-girder, a conventional I-girder specimen as shown in Fig. 2 is also designed. The new and the conventional I-girders are named with SP-N and SP-C respectively. “SP” denotes “Specimen”, and “N” and “C” denote “New” and “Conventional” respectively. The span, the height and the flange width are all same for the two specimens. Considering the high out-of-plane bending stiffness of the corrugated web, the web thickness of SP-N is designed to be 3 mm while such value of SP-C is designed to be 6 mm. The detailed dimensions of the two specimens are tabulated in Table 1. For the trapezoidally corrugated web, its size is listed in Table 2.

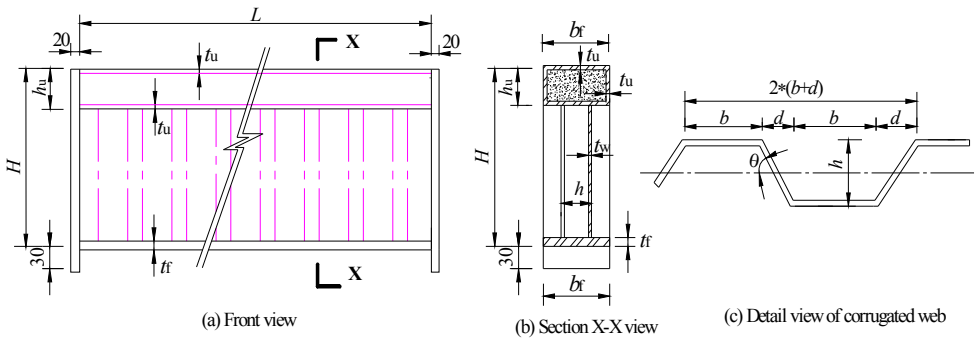

Fig. 1 A new I-girder with corrugated web and a concrete-filled tubular flange

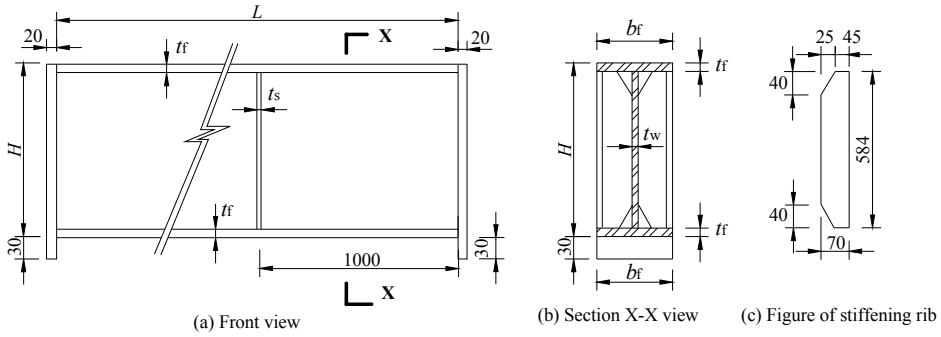

(a) Front view (b) Section X-X view (c) Figure of stiffening rib

Fig. 2 Conventional I-girder specimen (dimensions in unit of mm)

Table 1 Geometric dimensions of I-girder specimens

Specimen	L (mm)	H (mm)	t_f (mm)	b_f (mm)	t_w (mm)	t_s (mm)	t_u (mm)	h_u (mm)
SP-C	2000	600	8	160	6	6	-	-
SP-N	2000	600	6	160	3	-	3	80

Table 2 Geometric dimensions of trapezoidal web

Specimen	b (mm)	d (mm)	h (mm)	θ (^{o})
SP-N	110	90	90	45

Table 3 Properties of steel materials

Thickness t (mm)	f_y (MPa)	f_u (MPa)	e (%)	E (GPa)
8 (t_f)	252	450	29.5	200.0
6 (t_w)	280	457	29.3	193.4
3 (t_w)	394	559	21.6	197.5
3 (t_u)	377	491	21.4	210.0

The mechanical properties of the steel materials and the infilled concrete are measured from standard tests. The yield strength, the tensile strength, the elongation percentage and the elastic modulus of the steel plates with different values of thickness are obtained from uni-axial tensile tests of standard coupons. The test results are given in Table 3. For the concrete filled in the tubular flange, its compressive strength is measured from compressive tests on cubic specimens with a size of 150 mm × 150 mm × 150 mm. The characteristic value of the compressive strength is measured to be 31.2 MPa.

For both conventional and new I-girders, the flanges, the webs and the stiffeners are all connected together through welding. For the new I-girder, it is cured for a month after the concrete is filled into the tubular flange. At the ends of both specimens, steel plates with a thickness of 20 mm (namely end plates) are welded to both the flanges and the web. The end plates are 30 mm higher than the I-girders, and they are flush with the I-girder on the top surface. Therefore, the

bottom surface of the I-girder is higher than the bottom of the end plates (30 mm distance) to ensure that the specimens can rotate freely without contact with the supports at the ends during the test.

2.2 Test setup

The two specimens are tested in the test rig as shown in Fig. 3. A compressive machine with a maximum loading magnitude of 500 kN is used to apply concentrated load at the mid-span of the I-girders. The maximum displacement produced by the actuator is ±75 mm. The I-girder specimen is pinned at its both ends. As the length and the height of the two specimens are 2000 mm and 600 mm respectively, the specimens are mainly subjected to shear action when they are loaded at the mid-span because they have a small length-to-height ratio and a short span.

To monitor the failure process of the specimens, strain gauges are placed to measure the strain developments at some critical positions. For the conventional I-girder, the web is a flat-plate with a large slenderness, which causes it to be much sensitive to local buckling. Because the web of the specimen SP-C is mainly subjected to the shear action, a flexural deformation may occur in the inclined direction (approximately to be in an angle of 45° to the horizontal line). Therefore, strain

Fig. 3 Test setup

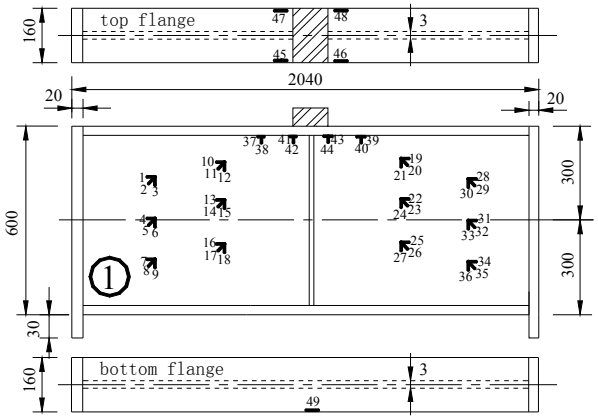

Fig. 4 Strain gauge placement for SP-C

gauges are placed on the web in the diagonal direction as shown in Fig. 4. To decrease the local effect of the concentrate load at the mid-span on the loading region, transverse stiffeners are placed symmetrically on the web at the mid-span. As seen from Fig. 4, a steel block is placed on the top flange at the mid-span of the I-girder to avoid a direct contact between the actuator and the top plate flange. On the top flange, four strain gauges (45-48) are arranged at the four corners of the steel block to monitor the strains in the longitudinal direction and evaluate if local yielding or buckling failure may occur at these positions. At the mid-span, a strain gauge (49) is also placed on the bottom flange to monitor the strain development.

For the new I-girder, it is expected that no buckling occurs in the web because the corrugation can improve the out-of-plane bending stiffness. Based on this consideration, the strain gauges are mainly placed along the web height at the mid-span because this location is under the maximum bending moment. For a comparison, strain gauges along the web height are also arranged at the 1/4 of the span to monitor if local buckling occurs. The detailed placement of the strain gauges can be found in Fig. 5. On the top and the bottom flanges, strain gauges are placed in the longitudinal direction to monitor the normal strain developments. It is noted that strain gauges are placed on the two surfaces of the web symmetrically, and hence "①" and "②" denote such two surfaces respectively.

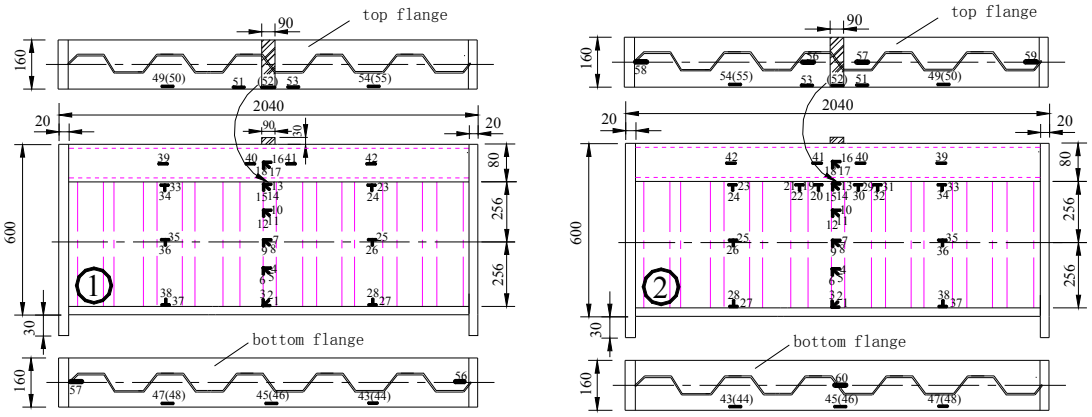

Fig. 5 Strain gauge placement for SP-N

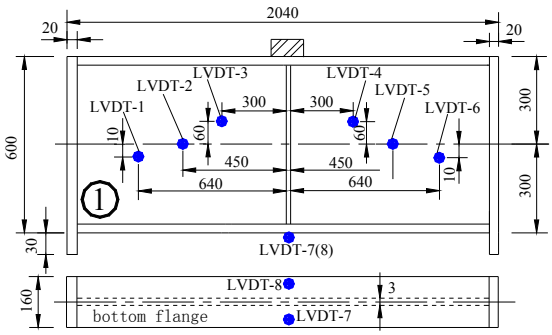

Fig. 6 LVDT placement for SP-C

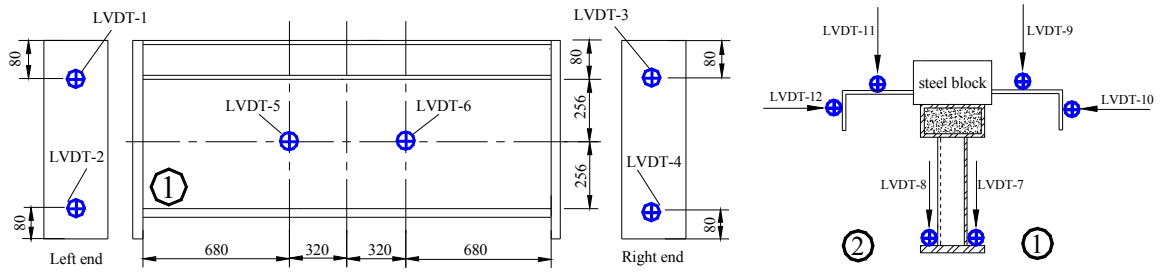

Fig. 7 LVDT placement for SP-N

To monitor the failure process, it is also necessary to measure the deformation of the specimens. Linear variable displacement transducers (LVDTs) are then placed at some positions to check the deformations at these locations. The placements of the LVDTs for both specimens are illustrated in Figs. 6 and 7 respectively. For the conventional I-girder, some LVDTs (LVDTS 1-6) are placed at some positions on the web to monitor if local buckling occurs during the loading process. These LVDTs are arranged in an inclined direction on the web to measure the flexural deformations at these locations. Additionally, two LVDTs (LVDTs 7-8) are placed on the bottom flange at the mid-span to monitor the deflection development. The two LVDTs are symmetrical to the center line of the plate flange, and they are also able to check if torsional deformation exists during the loading process.

For the new I-girder, it is expected to fail in flexural strength or shear strength rather than local buckling on the web. Based on this consideration, overall twelve LVDTs are placed on the specimen as shown in Fig. 7. LVDTs 1-4 are arranged at two positions of the end plates, and the two positions are close to the the top and the bottom ends of each end plate. They are used to monitor the rotations of the two end plates to check the actual boundary conditions for the specimen. LVDTs 5-6 are placed at the mid-height of the web at about two 1/3 points of the span to measure the out-of-plane displacement of the corrugated web to assess if buckling occurs here. To monitor if global buckling of the top concrete-filled tubular flange occurs, two LVDTs 10 and 12 are placed perpendicular to an L-shape steel plate connected to the steel block to measure the lateral displacement. LVDTs 7-9 and 11 are arranged on the bottom flange and on the top flange respectively to measure the deflection of the specimen.

3. Test results and discussion

3.1 Failure mode

For conventional I-girder specimen, the concentrated load at the mid-span is increased with an increment of 0.5 mm/min. When the concentrated load is about 123 kN, local buckling occurs suddenly in the flat-plate web with a loud sound. Local buckling occurs in a half of the web as shown in Fig. 8. The flexural deformation due to local buckling is at an approximate 45° line along the diagonal direction, which indicates that the buckling mode is caused by shear action. However, the concentrated load can be still increased after this local buckling, and it implies that post-buckling strength exists in this girder. When the load reaches a critical value of about 280 kN, it cannot be increased any more. At this moment, the test is stopped. After the test, it is observed that

no remarkable lateral deformation for the specimen as shown in Fig. 9, and it indicates that no global buckling occurs in the specimen.

For the new I-girder specimen, no any sudden buckling is observed during the loading process. After the concentrated load reaches 415 kN, the specimen cannot be loaded. The specimen after test shows a flexural deformation as shown in Fig. 10. It is found that the corrugated web just under the loading position has a large deformation as shown in Fig. 11. Simultaneously, the tubular flange has remarkable plastic deformation at the two sides of the steel block as shown in Fig. 12. The top tubular flange is cut off to observe the failure mode of the infilled concrete, and two inclined cracks can be found in the concrete under the patch loading location as shown in Fig. 13. Such inclined cracks indicate that the infilled concrete has a shear failure.

3.2 Load- strain curves for specimen SP-C

As seen from Fig. 8, local buckling of the web at one half is the failure mode for specimen SP-C. At buckling, the web under maximum compression in principal direction flexures. To study the

Fig. 8 Local buckling in web of SP-C

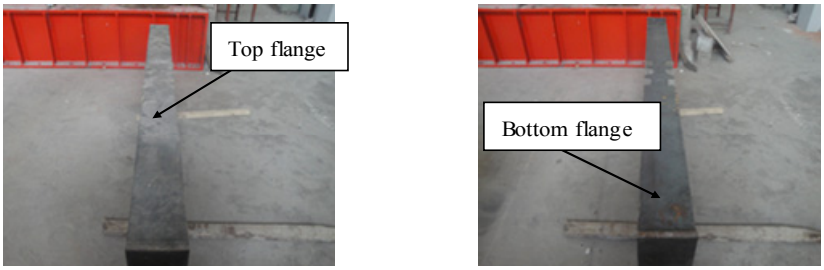

Fig. 9 Deformation in flange of SP-C

Fig. 10 Flexural deformation of SP-N

Fig. 11 Local deformation of corrugated web

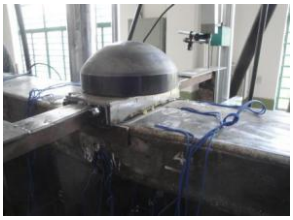

Fig. 12 Local deformation of tubular flange

Fig. 13 Inclined cracks in concrete

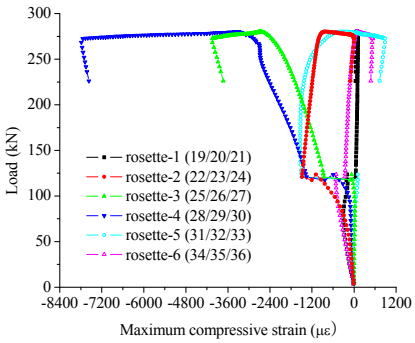

(a) Load-maximum compressive strain curves on web with buckling

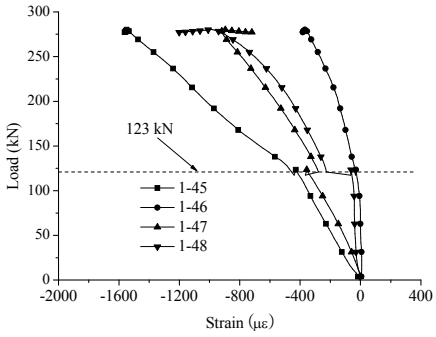

(b) Load-normal strains on top flange

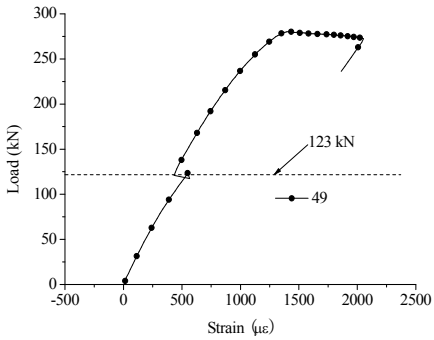

(c) Load-normal strains on bottom flange

Fig. 14 Load-strain curves of specimen SP-C

buckling mechanism clearly, the minimum normal strains, i.e., the minimum principal strain calculated from measured strains of the strain rosettes placed on the web in Fig. 4, are calculated and plotted in Fig. 14(a). As the right half of the web in the experimental test fails due to buckling, only the maximum compressive strains of the six strain rosettes on the right half of the web are plotted in Fig. 14(a). It is clear that the maximum compressive strains at the specified locations of the strain rosettes increase approximately linearly before the load reaches 123 kN. At a load of 123 kN, the maximum compressive strains have a sharp increase to indicate that large deformation occurs suddenly at these positions, which is caused by sudden local buckling of the web as seen in Fig. 8. It is also noted that the maximum compressive strains can still increase after local buckling of the web due to post-buckling strength. At a load about 280 kN, SP-C fails finally.

Strain gauges are placed on the top surface of the top flange to measure the strain developments at some positions close to the mid-span, and the measured normal strains are shown in Fig. 14(b). Because the top flange is under compression, the strains at the four locations are negative. At the critical load of 123 kN (web buckling), the normal strains are all much smaller than the yielding strain. Hence, the top flange is still in elastic strange at web buckling. After 123 kN, the normal strains increase continuously due to post-buckling strength of the web. At a load of about 280 kN, SP-C fails finally.

Similar strain development can be found in the strain gauge "49" placed on the bottom surface of the bottom flange in Fig. 14(c). The only difference is that the normal strain is positive due to tension. A normal strain jump also occurs at the web buckling and the specimen can still sustain the applied load due to post-buckling strength of the web. The final failure load is also about 280 kN, which is coincident with the measured results as shown in Figs. 14(a) and (b).

3.3 Load-longitudinal strain curves for specimen SP-N

For the new I-girder specimen SP-N, the load-longitudinal strain developments at some critical positions are plotted in Figs. 15(a)-(g). The strains placed along the web height at the mid-span are shown in Fig. 15(a). Except position 13, the strains at all other locations are very small before the load reaches the ultimate value of 415 kN, which implies that the corrugated web has very little contribution to the longitudinal tension or compression (i.e., weak resistance to bending moment). The strains at position 13 seem to increase faster because this location is just under the concentrated load, and it may be influenced by the effect of local stress concentration. The strain developments along the web height at 1/4 of the span are plotted in Fig. 15(b). All the strains increase in approximately linear tendency during the test even the load exceeds its ultimate value of 415 kN. The strains at all the positions are always in elastic state because their maximum values are smaller than the yielding strain.

The strains shown in Fig. 15(c) are measured from the strain gauges placed on the web's top. These strain gauges are just under the top concrete-filled tubular flange and close to the mid-span. The measured strains indicate that position 13 is under tension during the loading process, which implies initial imperfection exists at this location because this position should be subjected to compression in theory. At a loading about 350 kN, the positive strain at this position increases rapidly till it exceeds the yielding limit. At the peak load of 415 kN, the strains at most locations have a sharp change instantly. It is because local buckling occurs suddenly due to a large compression, and the experimental observations in Fig. 11 also support this conclusion.

The deformation of the top tubular flange can be evaluated from the strain developments on their side surface as shown in Fig. 15(d). The side surface of the top flange is subjected to compression because the strains are all negative. However, it is clear that the compressive strains at points 39 and 42 are very slight during the entire loading process, which indicates that the mid-height on the side surface of the top tubular flange is close to the neutral axis of the specimen under bending action. The strains at other points 16, 40 and 41 are also very slight before the load reaches about 350 kN. After that load, it seems that the strains at these points develop very fast. This phenomenon can be explained due to the local deformation of the steel tube under the concentrated load because these points are all located around the loading position. When the concentrated load exceeds a critical value, local buckling or yielding occurs due to the thin-walled geometry of the steel tube, which can be observed from Fig. 12. In overall, the strains at the mid-height of the side surface are all very small when the load is not large, and such position is hence

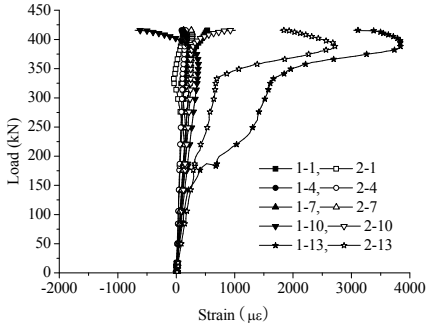

(a) Strains on web at mid-span

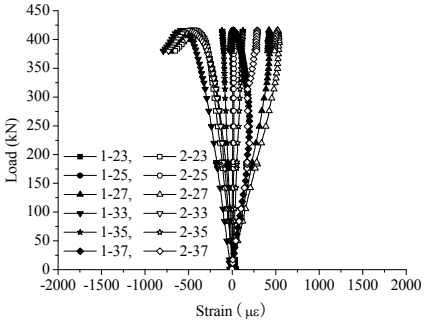

(b) Strains on web at 1/4 of span

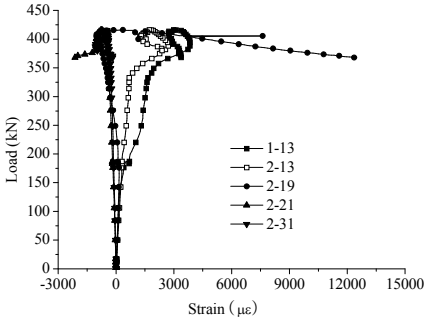

(c) Strains at web top under loading position

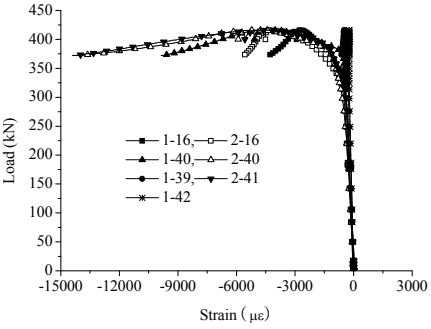

(d) Strains on side surface of top tubular flange

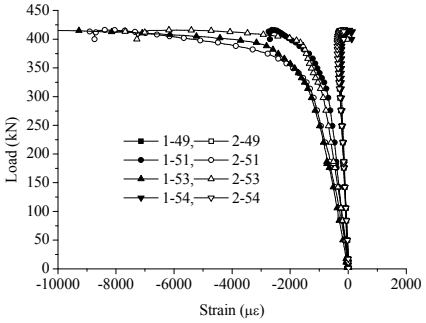

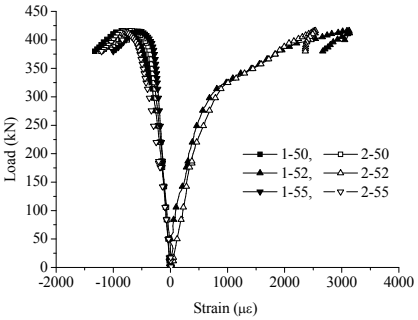

(e) Strains on top and bottom surfaces of top tubular flange

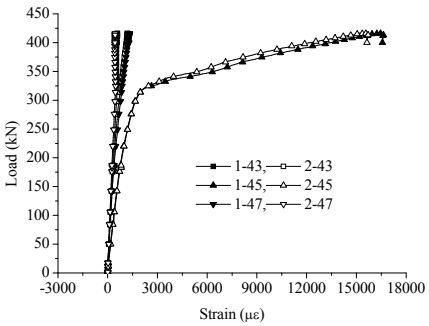

(f) Strains on bottom flange

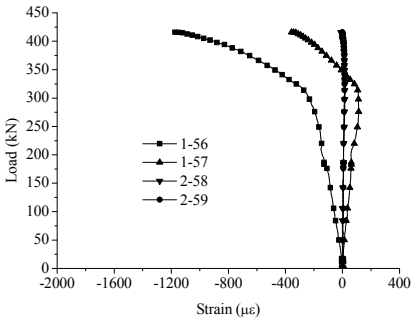

(g) strains at specimen's ends

Fig. 15 Load-longitudinal strain curves of specimen SP-N

close to the neutral axis of the new I-girder. This conclusion also proves that the corrugated web sustains relatively much smaller tension compared to the top concrete-filled tubular flange.

Fig. 15(e) provides the strain developments on the top and on the bottom surfaces of the top concrete-filled tubular flange. Positions 49, 51, 53 and 54 are located on the top surface and positions 50, 52 and 55 are located on the bottom surface. Positions 51, 53 and 52 are close to the loading position at the mid-span. Experimental results show that the strains at the positions far away from the loading position develop very slowly before the ultimate state. Influenced by local stress concentration, the strains at the positions close to the loading position increase much faster when the thin-walled steel tube has local buckling or yielding at a lower loading. However, such strains are still small before local failure occurs. It is also found that the strains at position 52 are positive, which indicates that the neutral axis is above the bottom surface of the top concrete-filled tubular flange because position 52 at the mid-span is subjected to the maximum bending moment in theory and it should be subjected to compression if the neutral axis is in the corrugated web.

The strain developments on the bottom flange are illustrated in Fig. 15(f) in which position 45 is located at the mid-span. Clearly, the bottom flange is under tension based on the observations of the positive strain values at these positions. Before the load reaches about 310 kN, the strains at the three positions increase linearly. After that loading value, the strain at position 45 increases much faster in a nonlinear tendency, which indicates that the position is in yielding state. However, the strains at positions 43 and 47 still increase linearly after the loading of 310 kN, and it is because the neutral axis moves upward to the top concrete-filled tubular flange and thus part of the top flange can sustain the tension to delay the fast strain developments at these positions.

Finally, the strains on the top and on the bottom flanges at both ends of the specimen are plotted together in Fig. 15(g). Positions 56 and 57 are placed on the bottom flange while positions 58 and 59 are arranged on the top flange. The positions of the four strain gauges are located at the ends of the specimen. The measured strains are used to check the actual boundary constraints. The strains at positions 58 and 59 are almost to be zero during the entire loading process, which implies that the top concrete-filled tubular flange has an ideal hinged boundary condition at its two ends. However, for the bottom flange, the strains become all negative at final loading stage to indicate that the rotations at the two ends of the bottom flange are subjected to some restrictions.

3.4 Load-transverse strain curves for specimen SP-N

The transverse strain development at the side surface of the top concrete-filled tubular flange is shown in Fig. 16(a). The strain increases gradually in the initial stage with the increase of the load. At a loading of about 350 kN, the transverse strain increases much quickly till it is beyond the yielding strain although the load is increased with a very slight magnitude. This is due to the occurrence of local buckling of the steel tube. Because the infilled concrete can avoid the concave deformation, the side surface of the steel tube has a convex deformation and its outer surface is then under tension, which coincides with the measured positive strains as shown in Fig. 16(a).

The transverse strains along the web height at the mid-span are plotted in Fig. 16(b). Under the concentrate compressive load, these strains are all negative and most of them increase linearly before the ultimate load. Even in the final stage, the strains seem to be still less than the yielding limit. However, the top of the web under the loading position has a severe plastic deformation as shown in Fig. 11. The measured strains in the final stage are less than the yielding strain because the strain gauges are not placed exactly on the folding corner. As shown in Fig. 11, the top of the web under the loading position is severely folded to form folding corner. At the folding corner,

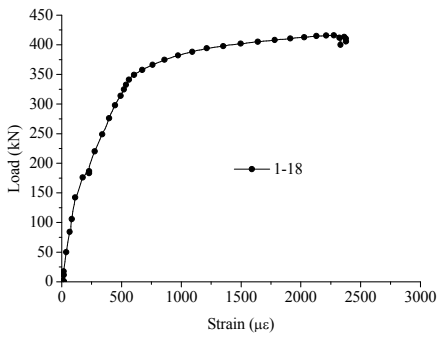

(a) Strain at side surface of top tubular flange

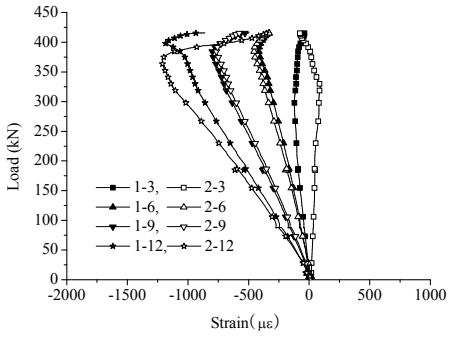

(b) Strains along web height at mid-span

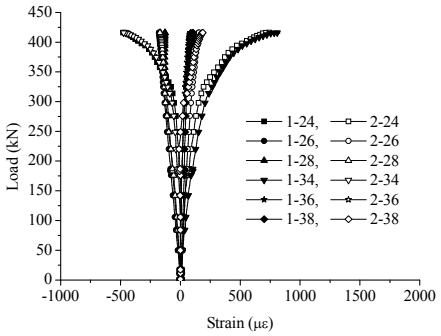

(c) Strains along web height at 1/4 of span

Fig. 16 Load-transverse strain curves of specimen SP-N

large plastic deformation is accumulated. However, the web is still close to be a plate far away from the folding corner. Therefore, the strains not located at the folding corner are not very big. It is also observed that the strain at position 3 is minimum while the strain at position 12 is maximum because position 3 is located at the bottom of the web and it is far away from the loading position on the top flange.

The strains along the web height at 1/4 of the span are illustrated in Fig. 16(c). The results indicate that most of the strains increase linearly during the entire loading process except the strains at positions 24 and 34 which are located on the top of the web. These two positions are influenced by the loading position where stress concentration exists. Even though the strain developments at positions 24 and 34 are not linear in the final stage, the strains are still far away from the yielding limit, and all the positions are always in elastic stage during the test.

3.5 Load-displacement curves for specimen SP-C

The deformation of the conventional I-girder specimen SP-C can be evaluated from the measured displacements at some critical positions. LVDTs 1-6 as shown in Fig. 6 are used to monitor the lateral displacements at some selected positions of the web. LVDTs 1-3 and LVDTs 4-6 are placed on the left half and on the right half of the web respectively. From the experimental observations, it is found that only half of the web is buckled as shown in Fig. 8, and LVDTs 4-6 are located on the buckled half. From Fig. 17(a), it can be seen that the lateral displacements of

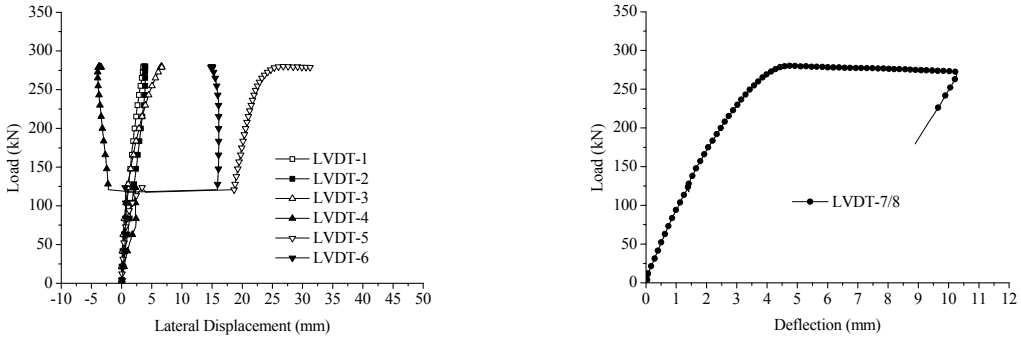

(a) Lateral displacement at web (b) Deflection at mid-span

Fig. 17 Load-displacement curves of specimen SP-C

LVDTs 1-3 are always very slight during the loading process, and such slight values of the lateral displacements at these positions are caused by the initial imperfection of the web. The measured results are coincident with experimental observations because no buckling occurs in this half of the web. For the lateral displacements measured from LVDTs 4-6, they have a sharp jump at the load of 123 kN, which implies that local buckling occurs at this moment, and this phenomenon is also coincident with the experimental observations.

In Fig. 17(b), the vertical displacement of the conventional I-girder specimen at the mid-span is plotted. The deflection increases gradually before the load of 280 kN. When the deflection increases to about 4.5 mm and the load is 280 kN, the specimen cannot sustain any load with the increase of the deflection, and the load begins to reduce after the peak point. The specimen then fails suddenly.

3.6 Load-displacement curves for specimen SP-N

The deformation of the new I-girder specimen SP-N is plotted in Figs. 18(a)-(d). In Fig. 18(a), the horizontal displacements of LVDTs 1-4 are illustrated. The locations of the four LVDTs are shown in Fig. 7, where LVDTs 1 and 3 are placed at the top flange and LVDTs 2 and 4 are placed at the bottom flange. The measured horizontal displacements at the four locations can be used to evaluate the rotation of the two ends of the specimen. It is clear that the displacements of LVDTs 1 and 3 increase much faster than the corresponding results of LVDTs 2 and 4, which indicates that the top flange of the specimen has a remarkable relative displacement in horizontal direction. The horizontal displacements of LVDTs 2 and 4 are quite minor, and it implies that the bottom flange is restrained in horizontal movement.

LVDTs 5 and 6 are placed at mid-height of the web at about two 1/3 points of the span to measure the lateral displacements of the web. The experimental results of the lateral displacements at the two positions are illustrated in Fig. 18(b). During the entire loading process, the lateral displacements at the two positions are always very minor although they increase slightly in the final stage. Such slight increase may be caused by the large local deformation at the top of the web at the mid-span as shown in Fig. 11. Generally, the out-of-plane deformation of the web, evaluated from the above lateral displacements, is very small, and no buckling occurs in the web except at the top of the web at the mid-span, where local buckling occurs because it is subjected concentrated load.

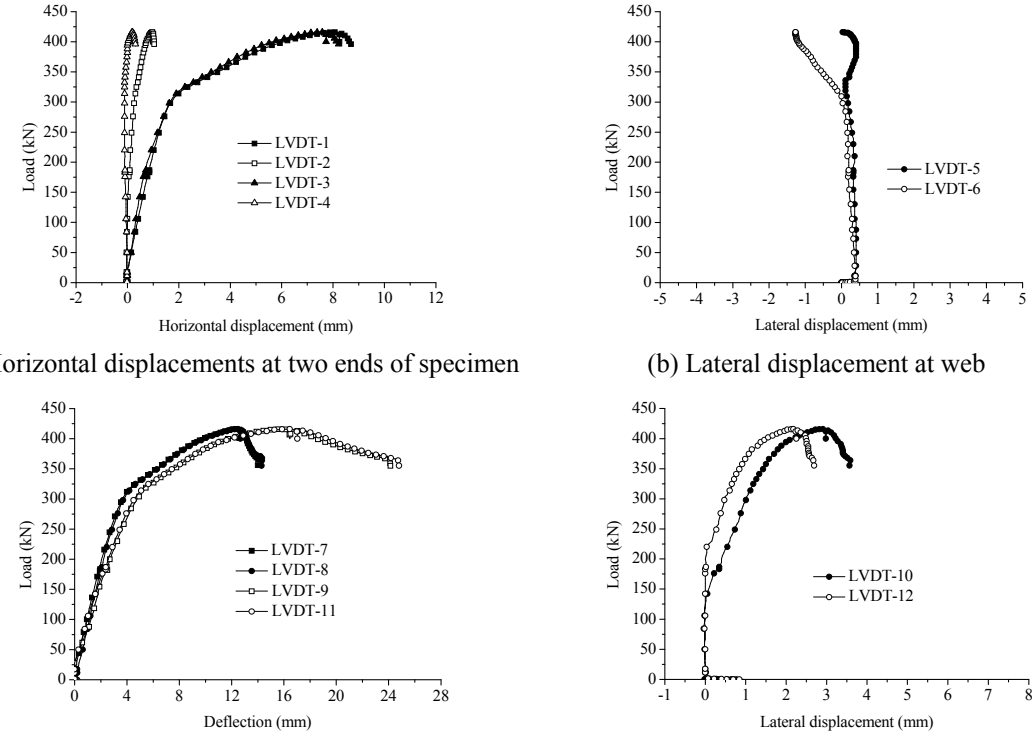

(a) Horizontal displacements at two ends of specimen

(b) Lateral displacement at web

(c) Deflection at mid-span

(d) Lateral displacement at top flange

Fig. 18 Load-displacement curves of specimen SP-N

The deflection of the specimen can be analyzed from the vertical displacement at the mid-span. Two LVDTs 7 and 8 are placed on the bottom flange and other two LVDTs 9 and 11 are placed on the top flange to measure the vertical displacement at the mid-span. The experimental results are shown in Fig. 18(c). The deflections of the top and the bottom flanges are very close. However, the top flange seems to have a larger deflection in final stage because the bottom flange yields firstly while the top flange has still a large potential before failure. For the top flange, the deflection at the maximum load is about 16 mm, which is much bigger than the serviceability limit. Obviously, the ductility of the new I-girder is much better than conventional plate I-girder since the deflection at peak load for the conventional I-girder specimen is only 4 mm.

LVDTs 10 and 12 are used to monitor the lateral displacement of the top flange. However, they are not placed on the two sides of the top flange. Actually, two L-shape steel plates as shown in Fig. 7 are welded to the steel block placed on the top flange. The LVDTs are placed on the vertical plate in the L-shape steel plate. During the test, the LVDTs are motionless and the L-shape steel plate moves downward together with the steel block and the flange. Therefore, there is a relative slip between the LVDT and the vertical plate. The L-shape steel plate will rotate if the top flange has a lateral displacement, which will cause the two LVDTs to have lateral displacements with different sighs (i.e., the two lateral displacements are in different directions). The experimental results of the lateral displacements measured from LVDTs 10 and 12 are shown in Fig. 18(d). It is clear that the lateral displacements of the two LVDTs are both close to be zero in the initial stage. When the load increases to certain value, the lateral displacements begin to increase. However, the

two lateral displacements are both increasing in same direction, i.e., the two lateral displacements are both positive. This phenomenon indicates that the lateral displacements are not produced due to the rotation of the top flange, and they are possibly caused by the following reason: The angles between the two plates in the L-shape steel plates as shown in Fig. 7 are both slightly smaller than 90^o. When the L-shape steels move downward with the top flange, the LVDTs slide upward on the surface of the vertical plate (actually it is not absolutely vertical as mentioned here). As the angles of the two plates in the L-shape steel plates are less than 90°, the LVDTs will measure positive lateral displacements due to the inclined plates. In this case, the measured lateral displacements are both positive. Because the developments of the two lateral displacements are much similar and in same sign, the rotation of the specimen can not occur. Finally, the lateral displacements are very slight (less than 4 mm) although they have positive values after certain load, which also implies no distorsional deformation occurs in the top concrete-filled tubular flange.

3.7 Comparison between conventional and new I-girder specimens

Based on the experimental tests for the conventional plate I-girder specimen and the presented new I-girder specimen, the failure mechanisms for the two specimens can be discussed as follows:

(1) For conventional plate I-girder with a short span, the web is mainly subjected to shear force when a concentrated load is applied at the mid-span of the specimen. Under such shear action, the web is much sensitive to buckling due to its slenderness and it buckles in an inclined direction with maximum compression. As a corrugated web has much higher out-of-plane bending stiffness, it has better shear resistance to prevent the buckling. In a new I-girder, the corrugated web cannot sustain tension or compression except at the region close to the web-flange connection due to the so-called “accordion effect”. This conclusion is proved from the measured strains as shown in Fig. 15(a). Except point 13 (very close to the connection of the corrugated web to the top flange), all other points have very slight strain values before final failure. It indicates that the corrugated web does not sustain tension or compression produced by the bending moment. Most of the bending moment is thus sustained by the two flanges. The flat-plate is very weak in resisting shear force, and most of the shear force is assigned to the corrugated web.
However, the top concrete-filled tubular flange in a new I-girder is generally much stronger in resisting tension or compression than the bottom flat-plate flange. When the bottom flat-plate flange is not appropriately designed in dimension to cause a remarkable difference of strength between the top and the bottom flanges, the neutral axis may move toward to the top flange severely. In such case, the potential of high strength of the concrete-filled tubular flange cannot be developed fully. This conclusion is proved in the reported study by the authors (Shao and Wang 2017).
Shao and Wang (2017) also presented the equation for predicting the location of the neutral axis in the new I-girder as follow

$$y_n = \frac{A_{f1} \cdot \left(H - h_u/2\right)}{A_{f1} + A_{f2}} \tag{1}$$

where y_n is the distance from the neutral axis to the surface of the bottom flange, A_{f1} and A_{f2} are the equivalent areas of the top and the bottom flanges respectively, and $A_{f1} = A_{st} + E_c / E_s \cdot A_{cc}$. A_{st} and A_{cc} are the areas of the steel tube and the concrete on the cross section

of the top concrete-filled tubular flange. E_c and E_s are the elastic modulus of the concrete and the steel respectively.

From Eq. (1), the neutral axis of the new I-girder is calculated to be 428 mm,which indicates that the neutral axis is very close to the top concrete-filled tubular flange although it is still located at the corrugated web. Due to this reason, the bottom flange yields firstly before the failure of the top concrete-filled tubular flange, and this conclusion is supported from experimental observation as shown in Fig. 19 in which the bottom flange has a clear deformation due to yielding.

In the study reported by Shao and Wang (2017), the tensile stress in the bottom flange can be calculated from the following equation

$$\sigma = \frac{My_n}{I_e} \tag{2}$$

where M is the bending moment and I_e is the equivalent moment of inertia, and it is calculated from the following equation

$$I_e = \left(I_{st} + I_{sc}\right) + E_c / E_s \cdot I_{cc} \tag{3}$$

where I_{st}, I_{sc} and I_{cc} are the moments of inertia about the neutral axis for the bottom flat-plate flange, the steel tube and the concrete in the top flange respectively.

From Eqs. (2)-(3), the value of the concentrated load P_y at the yielding of the bottom flange can be calculated, and the predicted result is P_y = 305 kN. As seen from Fig. 20, the predicted yield load is very close to the experimental result. The ultimate load is much bigger than the yield load because the tensile strength of the bottom flange is 457 MPa, which is much bigger than the yield strength of 280 MPa as seen in Table 3.

If the thickness of the bottom flat-plate flange is increased from 6 mm to be 12 mm, the amount of steel material used in the new I-girder is still less than that of the conventional I-girder by about 20%. In this case, the distance from the neutral axis to the surface of the bottom flange is 346 mm, which is slightly deviated from the mid-height of the I-girder to the top flange. The value of the yield load P_y is calculated again from Eqs. (2)-(3), and it is about 608 kN. Compared to the tested I-girder, the yield load is increased by about 100%. Therefore, appropriate design for the dimension of the bottom flat-plate flange is necessary

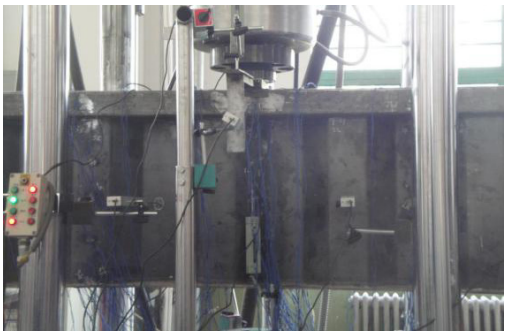

Fig. 19 Yielding of bottom flat-plate flange

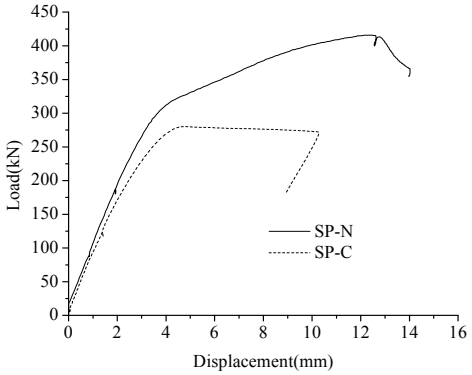

Fig. 20 Load-displacement curves of two I-girders

to develop the potential of high strength of the top concrete-filled tubular flange. The neutral axis is better to be located close to the mid-height of the girder. It is also pointed out that the stiffness in linear stage of the new I-girder is improved because the slope of the load-displacement curve for the new I-girder is clearly larger than that of the conventional one. The ductility of the new I-girder, which is evaluated from the maximum displacement at failure, is also better than that of the conventional one as seen in Fig. 20.

However, the corrugated web connected to the top flange at the mid-span may fail before the flexural yielding of the girder because local stress concentration produced by the concentrated load. The new I-girder in this study is observed to have this failure mode. In overall, the new I-girder specimen fails more possibly due to the tensile yielding at the bottom flange, or it may fail due to local failure at the top of the web under the patch loading on the top flange. In overall, the new I-girder behaves much more like a flexural beam.

(2) Although the conventional I-girder specimen has post-buckling strength after local buckling occurs in the web, it is disadvantageous for resisting fatigue or seismic action. Additionally, its final failure occurs at a very slight deflection after the peak load, which shows that the conventional I-girder has very little ductility. For the new I-girder, it has much better ductility because it fails due to the yielding strength of the bottom flange and yielding can produce much larger plastic deformation.

(3) The top concrete-filled tubular flange can improve the resistance for local compression, and it can also increase the lateral-torsional stiffness due to its closed section. Experimental observations show that the flat-plate flange is easy to be distorted with the buckling of the web as shown in Fig, 8. However, the distorsion of the concrete-filled tubular flange can be avoided due to two reasons: Firstly, the closed section of the steel tube has much bigger torsional stiffness. Secondly, the corrugated web enlarges the connecting height between the web and the flange in out-of-plane direction, which can also restrict the distorsion of the top flange. Experimental observations on the failure mode of the new I-girder support the above conclusions.

(4) The corrugated web in the new I-girder has very little capacity to resist tension or compression (the so-called accordion effect), and thus the bending moment is mostly sustained by the top and the bottom flanges. When the load tensile strength of the bottom plate flange (calculated from the product of the yield strength of the steel material and the

area of the cross section) is smaller than the compressive strength of the concrete-filled tubular flange (load carrying capacity of the combined steel tube and the infilled concrete), the neutral axis of the I-girder moves to the cross section of the top flange.

(5) As the two I-girder specimens fail due to different mechanisms, their load carrying capacities are also much different. The ultimate load of the new I-girder specimen (415 kN) is definitely larger than that of the conventional plate I-girder specimen (280 kN), and an increase of 48.2% is found in this study. It is also noted here that the bottom flange of the new I-girder is yielding while the top concrete-filled tubular flange still has much potential before yielding failure due to the combined action of both the steel tube and the infilled concrete. Based on a consideration of optimization, the bottom flange can be designed with a larger dimension to ensure that it can yield simultaneously with the top flange. This can be implemented without wasting amount of steel material because the corrugated web can be designed with a much smaller thickness compared to the flat-plate in conventional I-girders. In this case, the load carrying capacity will be improved more efficiently.

(6) The new I-girder is only suitable for application in bridge engineering when its both ends are hinged, i.e., no hogging moment exists in the girder. When the I-girder is used in building or other structures and one or both ends of the I-girder are fixed, hogging moment exists at some position along the length. In this case, the bottom flange is also necessary to be designed as a concrete-filled tubular one since a flat-plate flange is weak in resisting compression. The behavior of an I-girder with both top and bottom concrete-filled tubular flanges is suggested to be studied in the future. Additionally, the steel materials used in the new I-girder is only about 67% in amount compared to the steels used in the conventional I-girder. As seen from Fig. 21, the load carrying capacity of the new I-girder is still larger than that of the conventional one although the new I-girder can save about one-third amount of steel material. However, the steel tube in the concrete-filled tubular flange cannot be too small in size of cross section because it is very difficult to fill the concrete into the tube. A small size of cross section also causes the slenderness of the concrete-filled tube to be much larger, which leads to sensitivity of the concrete-filled tube to deformation in construction.

4. Conclusions

Through experimental tests on two different types of I-girders under shear action, the following conclusions can be obtained:

(1) Corrugate web has much higher resistance to buckling due to its high out-of-plane fexural stiffness. Local buckling can be prevented efficiently if suitable dimensions of corrugated web are selected.

(2) Replacing the flat-plate flange under compression in an I-girder with a concrete-filled tubular flange can improve the resistance to distorsion and to local load bearing capacity.

(3) For a conventional I-girder and a new I-girder with corrugated web and concrete-filled tubular flange, their mechanisms are much different when they have a short span and they are subjected mainly to shear action. The conventional I-girder is much sensitive to local buckling of the web due to its large slenderness in out-of-plane direction. However, the new I-girder behaves much more like a flexural beam, and flexural strength due to yielding is generally dominant.

(4) The new I-girder seems to have both higher load carrying capacity and better ductility compared to the conventional plate I-girder based on the experimental results.

References

Abbas, H.H., Sause, R. and Driver, R.G. (2006), "Behavior of corrugated webs I-girders under in-plane loading", *J. Eng. Mech., ASCE*, **132**(8), 806-814.

Abbas, H.H., Sause, R. and Driver, R.G. (2007), "Analysis of flange transverse bending of corrugated web I-girders under in-plane loads", *J. Struct. Eng., ASCE*, **133**(3), 347-355.

Anapayan, T., Mahendran, M. and Mahaarachchi, D. (2011), "Lateral distortional buckling tests of a new hollow flange channel beam", *Thin-Wall. Struct.*, **49**(1), 13-25.

Anapayan, T. and Mahendran, M. (2012), "Improved design rules for hollow flange sections subject to lateral distortional buckling", *Thin-Wall. Struct.*, **50**(1), 128-140.

Avery, P., Mahendran, M. and Nasir, A. (2000), "Flexural capacity of hollow flange beams", *J. Constr. Steel Res.*, **53**(2), 201-223.

Basher, M., Shanmugam, N.E. and Khalim, A.R. (2011), "Horizontally curved composite plate girders with trapezoidally corrugated webs", *J. Constr. Steel Res.*, **67**(6), 947-956.

Driver, R.G., Abbas, H.H. and Sause, R. (2006), "Shear behavior of corrugated web bridge girders", *J. Struct. Eng., ASCE*, **132**(2), 195-203.

Dong, J. and Sause, R. (2009), "Flexural strength of tubular flange girders", *J. Constr. Steel Res.*, **65**(3), 622-630.

Elgaaly, M. and Seshadri, A. (1997), "Girders with corrugated webs under partial compressive edge loading", *J. Struct. Eng., ASCE*, **123**(6), 783-791.

Elgaaly, M., Hamilton, R.W. and Seshadri, A. (1996), "Shear strength of beams with corrugated webs", *J. Struct. Eng., ASCE*, **122**(4), 390-398.

Elgaaly, M., Seshadri, A. and Hamilton, R.W. (1997), "Bending strength of steel beams with corrugated webs", *J. Struct. Eng., ASCE*, **123**(6), 772-782.

Gao, F., Zhu, H.P. and Zhang, D.H. (2014), "Experimental investigation on flexural behavior of concrete-filled pentagonal flange beam under concentrated loading", *Thin-Wall. Struct.*, **84**, 214-225.

Guo, T. and Sause, R. (2014), "Analysis of local elastic shear buckling of trapezoidal corrugated steel webs", *J. Constr. Steel Res.*, **102**, 59-71.

Hassanein, M.F. and Kharoob, O.F. (2010), "Shear strength and behavior of transversely stiffened tubular flange plate girders", *Eng. Struct.*, **32**(9), 2617-2630.

Hassanein, M.F. and Kharoob, O.F. (2012), "An extended evaluation for the shear behavior of hollow tubular flange plate girders", *Thin-Wall. Struct.*, **56**, 88-102.

Hassanein, M.F. and Silvestre, N. (2013), "Lateral–distortional buckling of hollow tubular flange plate girders with slender unstiffened webs", *Eng. Struct.*, **56**, 572-584.

Heldt, T.J. and Mahendran, M. (1997), "Lateral-distortional buckling of hollow flange beams", *J. Struct. Eng., ASCE*, **123**(6), 695-702.

Ibrahim, S.A. (2014), "Lateral torsional buckling strength of unsymmetrical plate girders with corrugated webs", *Eng. Struct.*, **81**(12), 123-134.

Ibrahim, S.A., El-Dakhakhni, W.W. and Elgaaly, M. (2006), "Behavior of bridge girders with corrugated webs under monotonic and cyclic loading", *Eng. Struct.*, **28**(14), 1941-1955.

Kim, B. and Sause, R. (2008), "Lateral torsional buckling strength of tubular flange girders", *J. Struct. Eng., ASCE*, **134**(6), 902-910.

Kövesdi, B., Braun, B., Kuhlmann, U. and Dunai, L. (2010), "Patch loading resistance of girders with corrugated webs", *J. Constr. Steel Res.*, **66**(12), 1445-1454.

Kurniawan, C.W. and Mahendran, M. (2009), "Elastic lateral buckling of simply supported LiteSteel beams subject to transverse loading", *Thin-Wall. Struct.*, **47**(1), 109-119.

Luo, R. and Edlund, B. (1995), "Numerical simulation of shear tests on plate girders with trapezoidally

corrugated webs", Ph.D. Thesis; Division of Steel and Timeber Structures, Chalmers University of Technology, Sweden.

Luo, R. and Edlund, B. (1996a), "Ultimate strength of girders with trapezoidally corrugated webs under patch loading", *Thin-Wall. Struct.*, **24**(2), 135-156.

Luo, R. and Edlund, B. (1996b), "Shear capacity of plate girders with trapezoidally corrugated webs", *Thin-Wall. Struct.*, **26**(1), 19-44.

Machacek, J. and Tuma, M. (2006), "Fatigue life of girders with undulating webs", *J. Constr. Steel Res.*, **62**(1-2), 168-177.

Moon, J.H., Yi, J.W., Choi, B.H. and Lee, H.E. (2009), "Lateral-torsional buckling of I-girder with corrugated webs under uniform bending", *Thin-Wall. Struct.*, **47**(1), 21-30.

Nguyen, N.D., Kim, S.N., Han, S.R. and Kang, Y.J. (2010), "Elastic lateral-torsional buckling strength of I-girder with trapezoidal web corrugations using a new warping constant under uniform moment", *Eng. Struct.*, **32**(8), 2157-2165.

Sause, R. (2015), "Innovative steel bridge girders with tubular flanges", *Struct. Infrastruct. Eng.*, **11**(4), 450-465.

Sause, R. and Braxtan, T.N. (2011), "Shear strength of trapezoidal corrugated steel webs", *J. Constr. Steel Res.*, **67**(2), 223-236.

Sause, R., Kim, B. and Wimer, M.R. (2008), "Experimental study of tubular flange girders", *J Struct. Eng.*, *ASCE*, **134**(3), 384-392.

Sayed-Ahmed, E.Y. (2005), "Lateral torsion-flexture buckling of corrugated web steel girders", *Proc. Inst. Civ. Eng. Struct. Build.*, **158**(1), 53-69.

Shao, Y.B. and Wang, Y.M. (2017), "Experimental study on static behavior of I-girder with concrete-filled rectangular flange and corrugated web under concentrated load at mid-span", *Eng. Struct.*, **130**, 124-141.

Yi, J.W., Gil, H.B., Youm, K.S. and Lee, H.K. (2008), "Interactive shear buckling behavior of trapezoidally corrugated steel webs", *Eng. Struct.*, **30**(6), 1659-1666.

BU